Detecting Drizzle in Marine Warm Clouds Using Visible, Infrared, and Microwave Satellite Data

H. Shao and G. Liu
Florida State University
Tallahassee, Florida

Introduction

Determining the radiative effects of aerosols is one of the most important areas in climate research. There are observational evidences showing that aerosols can affect the radiative balance of the earth indirectly - as the number of aerosols increases, water in the cloud spreads over many more particles. Large concentrations of small droplets not only make the cloud more reflective, but also reduce the probability of rainfall and prolong cloud lifetime, because small droplets have less efficiency of coalescence (e.g., Albrecht 1989, Rosenfeld 2000). Since precipitation is a key component in determining the lifetime and extent of clouds, understanding to what extent that drizzle is suppressed in the polluted cloud in global scale is essential to assess this aerosol indirect effect. Global measurements require satellite observations, which cover much broader area and much longer time period than aircraft or surface based measurements. However, there have been very few studies on detecting drizzle from satellite. In this study, we present a satellite-measurable drizzle index (DI).

Drizzle Index

Observations showed that within a cluster of warm clouds, non-drizzling clouds satisfy $r_e(t) = ft^k$ (Martin et al. 1994, Szczodrak et al. 2001), where t is in-cloud optical depth varying from t = 0 (at cloud base) to $t = \tau$ (at cloud top), $r_e(t)$ is cloud effective radius (r_e) at optical depth t, f is cloud-dependent variable, and k is approximately constant. Integrating $r_e(t)$ from cloud base to top, we can express liquid water path (LWP) in terms of r_e at cloud top (r_e^{top}) and cloud optical depth (τ) without f explicitly appearing in the equation,

$$\mathrm{LWP} = \frac{2}{3+3k} r_e^{top} \tau \qquad (1)$$

Since f (a function cloud droplet number concentration) is much more variable than k (associated with cloud thermal-dynamic process), Eq. (1) is independent of f, indicating that within the same cloud cluster the relation among LWP, r_e^{top}, and τ are relatively constant during cloud developing stage. This fact is one of our bases for drizzle detection. To illustrate it, we assumed four different clouds as shown in Figure 1. Cloud 1, Cloud 2, and Cloud 3 are the same cloud but in different stage. Cloud 3 and Cloud 4 are different clouds in different stage but have the same r_e^{top} and τ. Their corresponding LWP, r_e at cloud top, and cloud optical depth are given by LWP_i, $r_e^{top}{}_i$, t_i, where i = 1, 2, 3, 4.

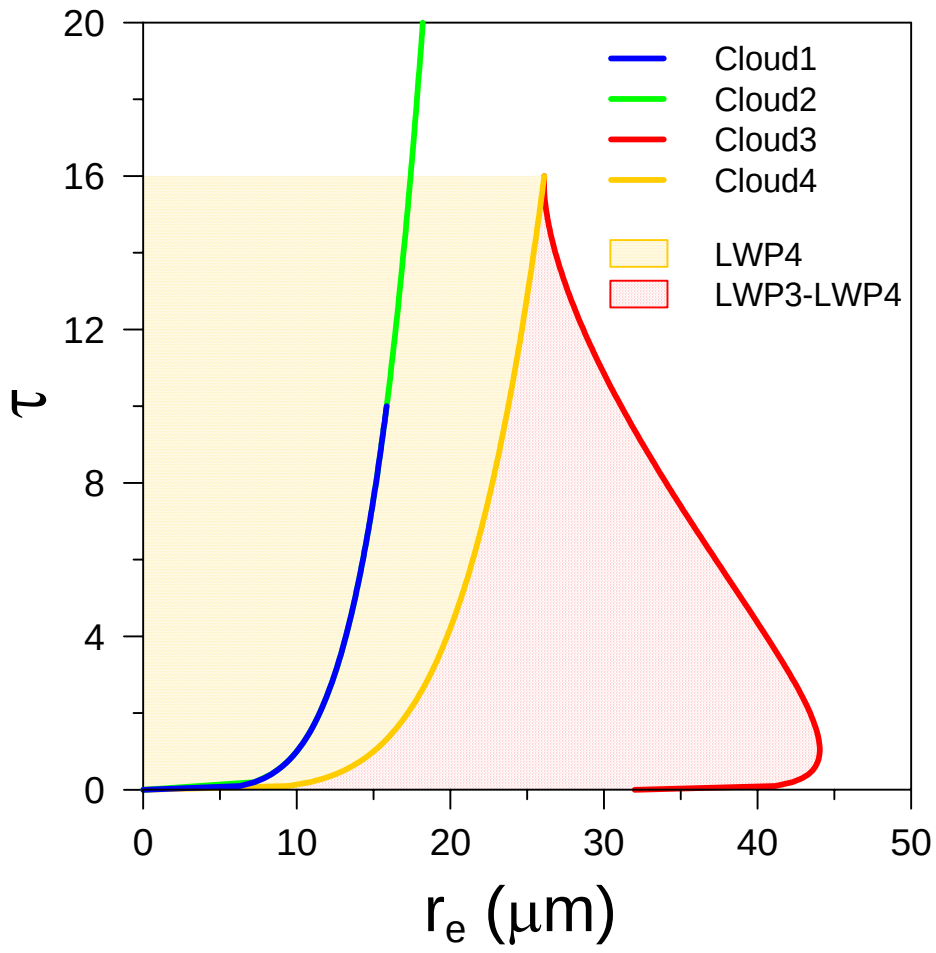

Figure 1. Schematic diagram of cloud r_e profile for different clouds. Cloud 1, Cloud 2, and Cloud 3 are the same cloud but in different developing stage. Cloud 1 is in early developing stage, Cloud 2 is in well developing stage, and Cloud 3 is in drizzling stage. Cloud 4 is another non-raining cloud but with the same r_e^{top} and τ as Cloud 3.

According to Eq. (1), also noting that $r_e^{top}{}_3 = r_e^{top}{}_4$ and $\tau_3 = \tau_4$, we have,

$$\frac{(3+3k)LWP_1}{2r_e^{top}{}_1 \cdot \tau_1} = \frac{(3+3k)LWP_2}{2r_e^{top}{}_2 \cdot \tau_2} = \frac{(3+3k)LWP_3}{2r_e^{top}{}_3 \cdot \tau_3} = 1, \quad \frac{(3+3k)LWP_4}{2r_e^{top}{}_4 \cdot \tau_4} = \frac{LWP_4}{LWP_3} > 1 \qquad (2)$$

Therefore, we introduce the drizzle index as defined by (Shao and Liu, 2004)

$$DI = \frac{(3+3k)LWP}{2r_e^{top}\tau} \approx \frac{LWP_m}{\alpha r_e^{\beta} \tau^{(3\beta-1)/2}} \qquad (3)$$

where, LWP_m is LWP derived from microwave measurements, r_e is satellite measured cloud r_e at near-infrared wavelength, τ is satellite measured optical depth at visible wavelength. Since satellite measured

r_e is somehow close to (but not equal to) r_e^{top}, in practice, we use $\alpha r_e^{\beta}\tau^{(3\beta-1)/2}$ instead, where α and β are regression coefficients determined by the relation $\ln LWP_m+0.5\ln\tau = \beta(\ln r_e-1.5\ln\tau)+\ln\alpha$ for those non-raining clouds that satisfy r_e <15 μm and $0.96 < (r_e\tau)/LWP_m < 1.2$. Based on this definition, for non-drizzle clouds, DI ≈ 1, no matter what cloud droplet number concentration they have or what developing stage they are in. For drizzling clouds, DI >1.

Model Simulation

Three groups of clouds with linear r_e profiles are simulated to examine the capacity of DI. They are: (1) non-drizzling clouds, (2) light drizzling clouds, and (3) drizzling/raining clouds. For non-drizzling clouds, r_e at cloud base (r_e^{btm}) is assigned to be 2 μm; r_e at cloud top (r_e^{top}) varies from 6 to 12 with 2 μm increments. For light drizzling clouds, r_e^{btm} is assigned to be 8 μm; r_e^{top} varies from 10 to 16 with an increment of 2 μm. For drizzling/raining clouds, r_e^{top} is assumed to be 12 μm, and r_e^{btm} varies from 12 to 18 μm with an increment of 2 μm. In the non-drizzle and light drizzle cases, τ (at 0.55 μm) is 8, 12, 18, 26, or 36. In the drizzle/rain case, τ (at 0.55 μm) is 6, 8, 12, 18, or 26. Using Santa Barbara discrete ordinate radiative transfer (DISORT) atmospheric radiative transfer model (Ricchiazzi et al. 1998) and the microwave radiative transfer model of Liu (1998), we calculated the upwelling radiances at the top of the atmosphere at visible (0.63 μm), near-infrared (1.61 μm) and microwave wavelengths (19 and 37 GHz). These synthetic radiances are then used to "retrieve" LWP, r_e, and cloud optical depth, using the retrieval algorithms described in Shao and Liu, 2004.

Using the synthetic data for the above three kinds of clouds, the relation of $\log(LWP_m\tau^{1/2})$ and $\log(r_e\tau^{3/2})$ is shown in Figure 2, with lines connecting the points that have the same τ. The best-fitting line for non-drizzle clouds is shown in the figure with the thick line. Figure 2 indicates,

1. For non-drizzle case, points are close to the fitting line. As τ increases points are almost parallel to the fitting line;

2. For light drizzle case, points are far away from the fitting line, and the departure increases as r_e^{top} decreases;

3. For drizzle/rain case, points are further away from the fitting line, and the departure increases as r_e^{btm} increases.

Also from Figure3, where their DI is measured by the departure from the line $LWP_c = LWP_m$ (here LWP_c is LWP calculated by $\alpha r_e^{\beta}\tau^{(3\beta-1)/2}$), it can be seen:

1. For non-drizzling clouds, DI is insensitive to cloud r_e profiles and varies from 0.9 to 1.1;

2. For drizzling clouds, as particles become larger (particularly near the cloud base), DI increases to beyond 1.1, and can be as large as 1.6.

We conclude that non-drizzle clouds can be adequately described by the relation of $LWP_m = \alpha r_e^{\beta} \tau^{(3\beta-1)/2}$, and DI is capable to reflect the change in particle size at cloud base.

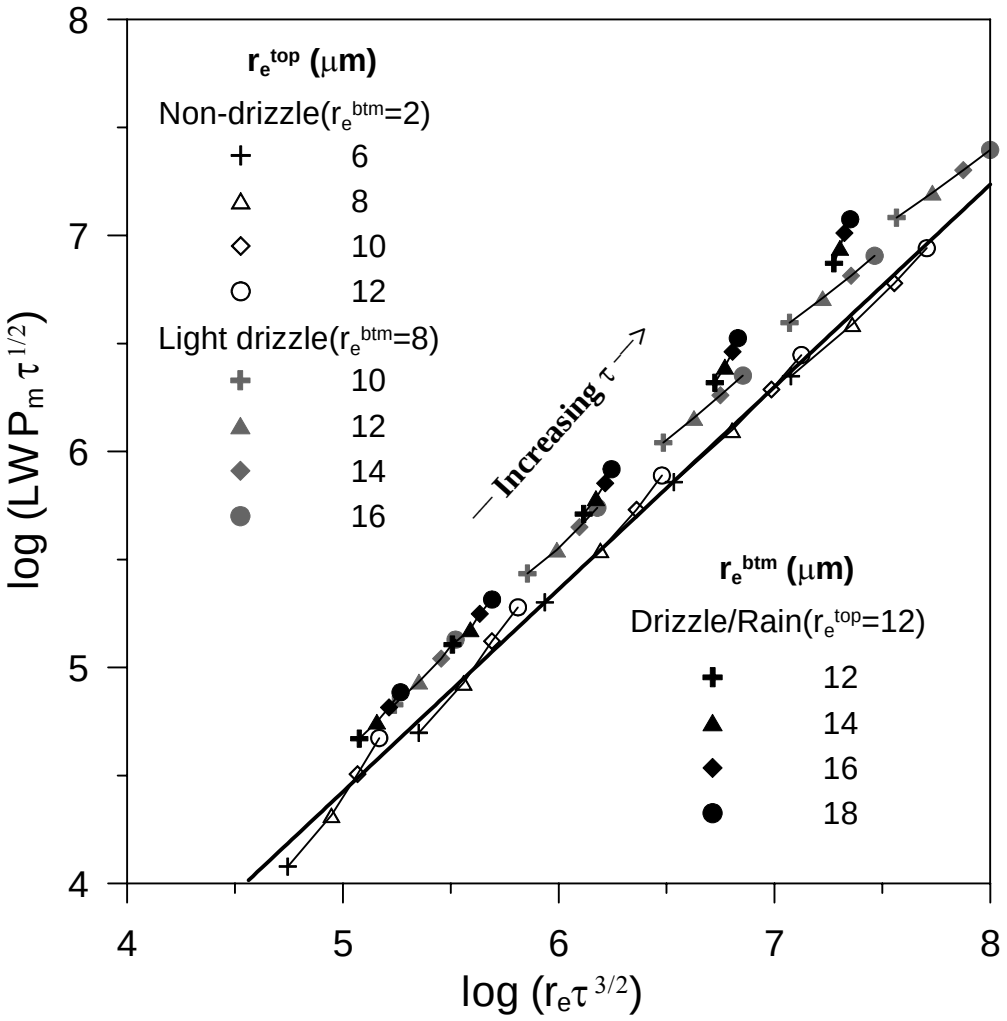

Figure 2. Relation between $\log(LWP_m\tau^{1/2})$ and $\log(r_e\tau^{3/2})$ as simulated by radiative transfer models. Units for LWP_m and r_e are $g \cdot m^{-2}$ and μm, respectively. Symbols denote the different r_e profiles as indicated in legend with a pair of effective radii at the top (r_e^{top}) and base (r_e^{btm}) of the cloud. The points with the same values of cloud optical depth are connected with thin lines. The thick line is the fitting curve for non-drizzling clouds.

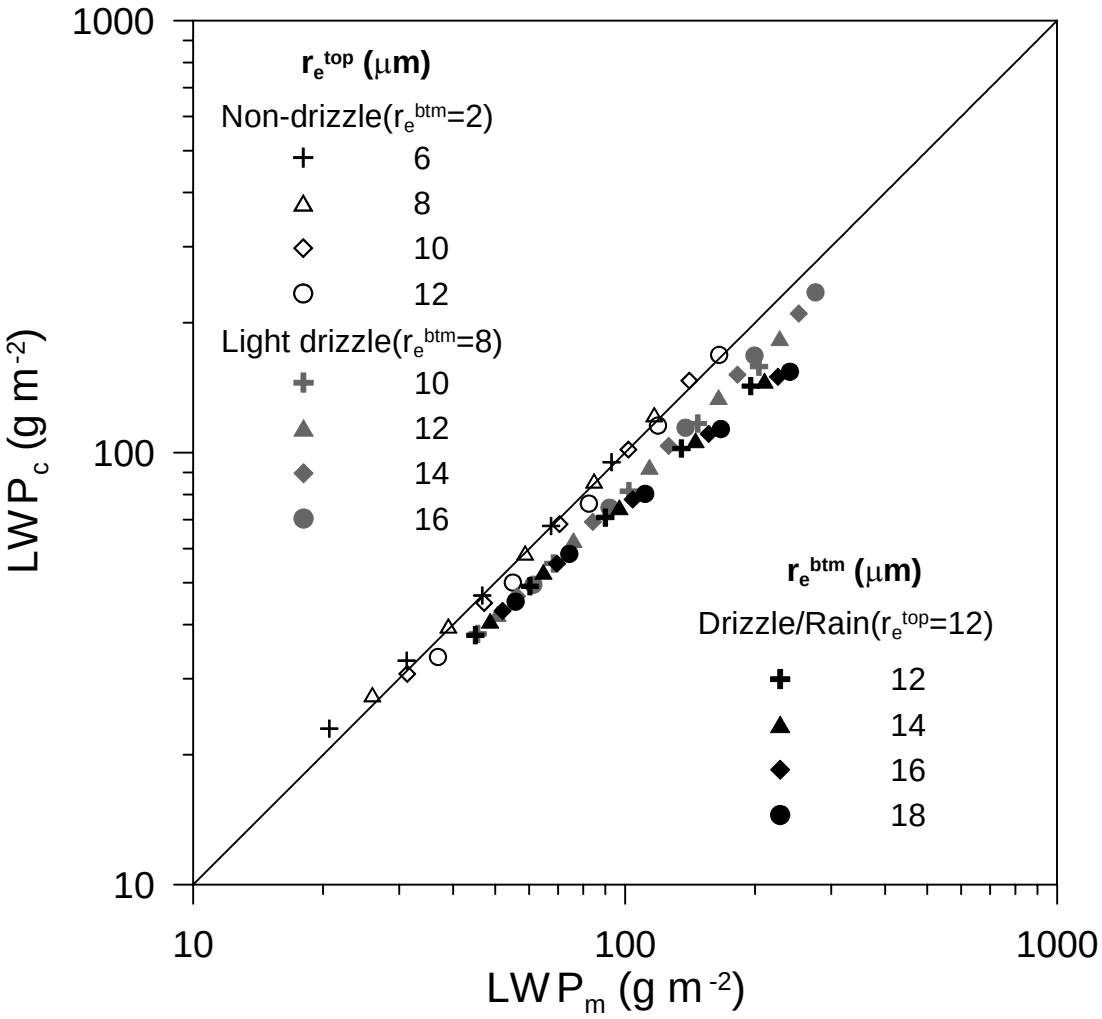

Figure 3. Scatter plot of LWP_c versus LWP_m. Symbols are the same as those in Figure 2.

Case Study

Case study is performed using Tropical Rainfall Measuring Mission measurements during the Dynamics and Chemistry of Marine Stratocumulus experiment on July 24, 2001. The reflectances at 0.63 μm and 1.61 μm visible infrared scanning radiometer (VIRS) channels are used to retrieve cloud optical depth and r_e at the solar wavelengths. Brightness temperatures at 19 and 37 GHz frequencies are used to derive cloud LWP in microwave range. Since the TMI has larger footprints than the VIRS, to collocate the measurements from the two sensors, we averaged VIRS-retrieved cloud effective radii and optical depths to create a new pixel that is centered at the TMI pixel center and has a footprint equivalent to the effective field of view of TMI 19.35 GHz. To avoid beam-filling error, only completely overcast pixels are selected. Additionally, pixels with cloud top temperature colder than 273 K are excluded in the analysis to avoid ice scattering.

Figure 4 shows the composite image with 0.63, 3.75, and 10.8 μm VIRS channels, horizontal distributions of the retrieved r_e and τ at VIR pixel resolution, and DI at TMI pixel resolution for the selected cases. From this figure, it is observed that

1. Clouds with large r_e but small τ also have large values of DI, consistent with the effect of drizzle formation that typically increase r_e and decrease τ (Nakajima and Nakajima 1995, Greenwald and Christopher 2000).

2. Large DIs are associated with those areas (enclosed by rectangle in Figure 4a) where clouds become broken and exhibit more cellular structures, consistent with the aircraft observations that suggested this pattern typically appeared in the region where drizzle was measured (Stevens et al. 2003).

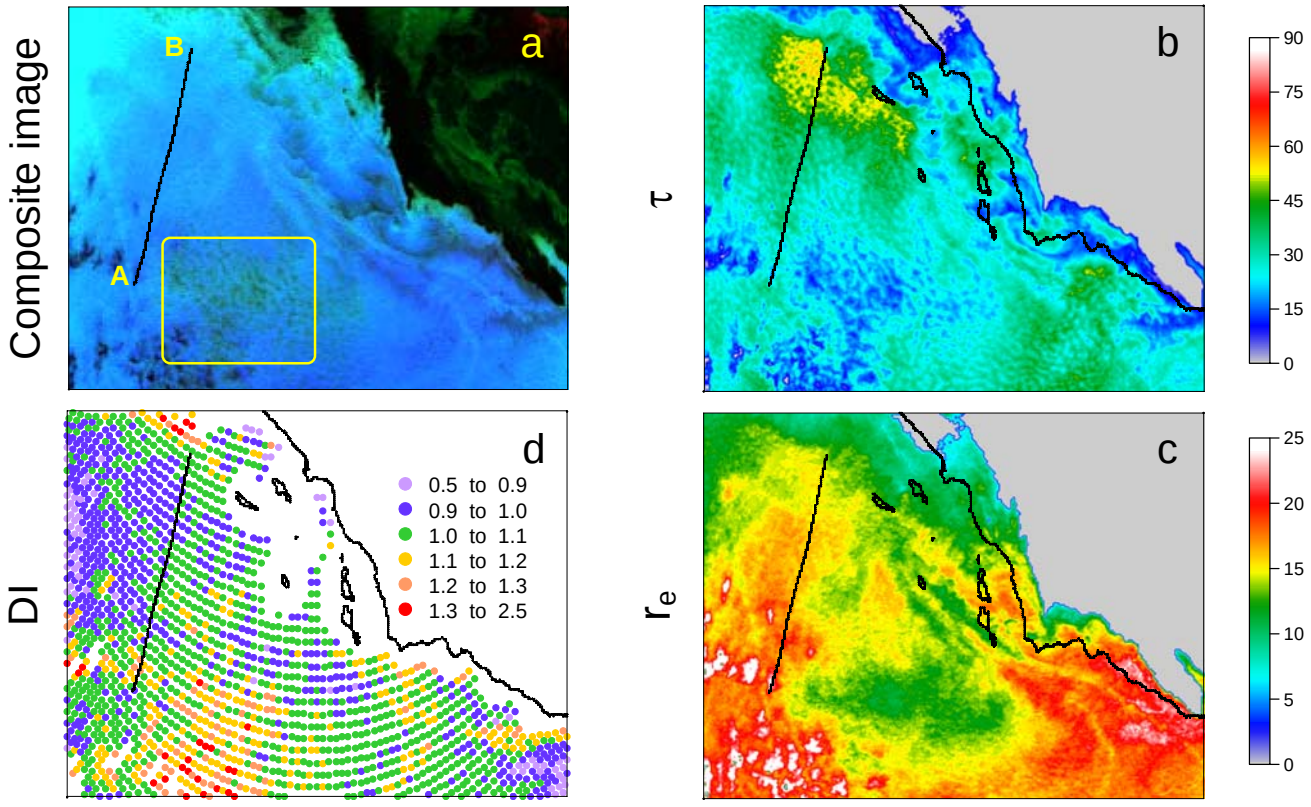

Figure 4. a) Composite satellite image with 0.63, 3.75, and 10.8 μm channels, b) horizontal distributions of τ, c) horizontal distributions of r_e, and d) horizontal distributions of DI. Line A-B indicates the flight track of C-130 aircraft.

Coincident measurements of Wyoming cloud radar equipped on C-130 aircraft are compared with our satellite assessment. Figure 5 shows radar reflectivity superimposed with DI and retrievals of r_e and τ along the line A-B shown in Figure 4a. The satellite passing time is indicated by dashed line. It is found that

1. DI peaks appear at almost the same position of the most intense reflectivity cells, where sudden changes in r_e and τ suggest the microphysical conditions in those cells are different from their surroundings;

2. DI~1.1 corresponds to r_e around 14 ~16 μm, consistent with the drizzle threshold of r_e ~15 μm used by others (e.g., Rosenfeld 2000, Masunaga et al. 2002).

Therefore, DI can be applied to satellite measurement for drizzle detection, and suggests that DI ~1.1 may be used for drizzle threshold, which is also consistent with our model simulations.

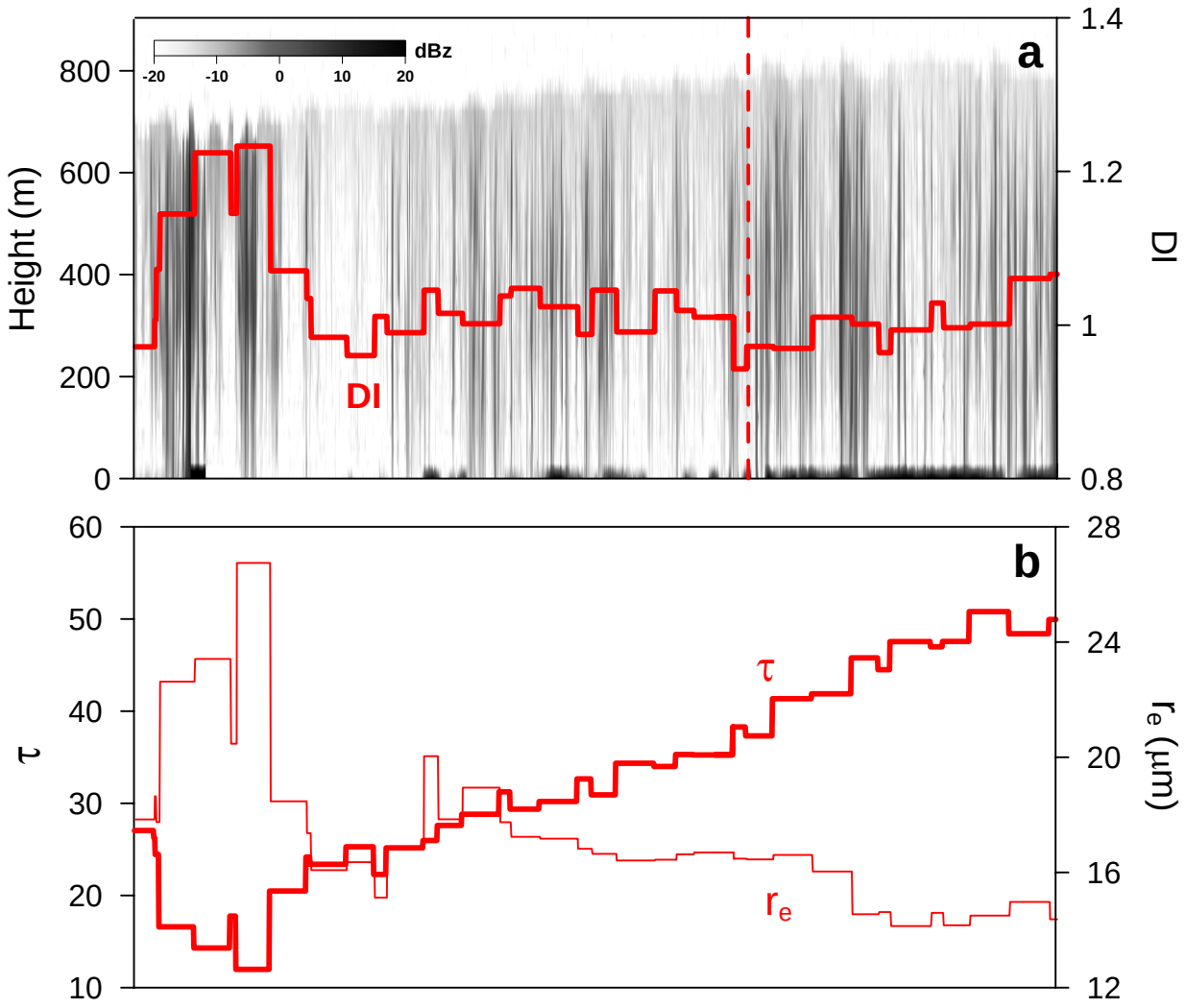

Figure 5. The time-height cross section of the radar reflectivity and satellite retrievals along the line A-B shown in Figure 4a. (a) Radar reflectivity superimposed with DI. Indicated by dashed line is satellite passing time; (b) retrievals of r_e and τ along line A-B.

Conclusion

We presented a method to detect drizzle in marine warm clouds by combining visible, near-infrared, and microwave measurements. The drizzle detection is based on the following two considerations: First, for warm non-raining cloud, $\alpha r_e^{\beta}\tau^{(3\beta-1)/2}$ is a good estimate of cloud LWP; second, drizzle formation changes cloud microphysical properties and vertical droplet size distribution, and accordingly alters the relation among LWP, optical depth, and r_e. This change results in a larger DI for drizzle clouds than for non-drizzle clouds. Model simulation and satellite observation show that DI is useful in differentiating between drizzle and non-drizzle clouds, and suggest that DI ~1.1 may be used for drizzle threshold.

Corresponding Author

Hongfei Shao, soar@met.fsu.edu, (850) 645-5629

References

Albrecht, B. A., 1989: Aerosols, cloud microphysics and fractional cloudiness. *Science*, **245**, 1227-1230.

Greenwald, T. J., S. A. Christopher, and J. Chou, 1996: SSM/I and GOES-8 comparisons of cloud liquid water path over water: assessment of sub-field of view effects in microwave retrievals. *J. Geophys. Res*, **102**, 19,585–19,596.

Liu, G., 1998: A fast and accurate model for microwave radiance calculations. *J. Meteorol. Soc. Japan*, **76**, 335–343.

Martin, G. M., D. W. Johnson, and A. Spice, 1994: The measurement and parameterization of effective radius of droplets in the warm stratocumulus clouds. *J. Atmos., Sci.*, **51**, 1823–1842.

Masunaga, H., T. Y. Nakajima, T. Nakajima, M. Kachi, R. Oki, and S. Kuroda, 2002: Physical properties of maritime low clouds as retrieved by combined use of Tropical Rainfall Measurement Mission Microwave Imager and Visible/Infrared Scanner: Part I, Algorithm. *J. Geophys. Res.*, **107**, 10.1029/ 2001 JD000743.

Nakajima, T. Y., and T. Nakajima, 1995: Wide area determination of cloud microphysical properties from NOAA AVHRR measurement for FIRE and ASTEX region. *J. Atmos. Sci.*, **52**, 4043–4059.

Ricchiazzi, P., S. Yang, and C. Gautier, 1998: SBDART: A practical tool for the plane-parallel radiative transfer in the earth's atmosphere. *Bull. Am. Meteorol. Soc.*, **79**, 2101-2114.

Rosenfeld, D., 2000: Suppression of rain and snow by urban and industrial air pollution. *Science*, **287**, 1793–1796.

Shao, H., and G. Liu, 2004: Detecting drizzle in marine warm clouds using combined visible, infrared, and microwave satellite data. *J. Geophys. Res.*, **109**, No. D7, D07205, 10.1029/2003 JD004286.

Stevens, B., et al., 2003: Supplement to dynamics and chemistry of marine stratocumulus—DYCOMS-II. *Bull. Am. Meteorol. Soc.*, **84**, 593–593.

Szczodrak, M., P. H. Austin, and P. B. Krummel, 2001: Variability of optical depth and effective radius in marine stratocumulus clouds. *J. Atmos. Sci.*, **58**, 2912–2926.